frontiers | Frontiers in Physics

TYPE Original Research
PUBLISHED 17 August 2023
DOI 10.3389/fphy.2023.1200601

OPEN ACCESS

EDITED BY
Sung-Kwan Mo,
Berkeley Lab (DOE), United States

REVIEWED BY
Wenlong Gao,
University of Paderborn, Germany
Botao Fu,
Sichuan Normal University, China

*CORRESPONDENCE
Gui-Bin Liu,
gbliu@bit.edu.cn

RECEIVED 05 April 2023
ACCEPTED 02 August 2023
PUBLISHED 17 August 2023

CITATION
Wang Y-R and Liu G-B (2023), Triply degenerate nodal line and tunable contracted-drumhead surface state in a tight-binding model.
Front. Phys. 11:1200601.
doi: 10.3389/fphy.2023.1200601

Triply degenerate nodal line and tunable contracted-drumhead surface state in a tight-binding model

Yi-Ru Wang[1,2] and Gui-Bin Liu[1,2]*

[1]Centre for Quantum Physics, Key Laboratory of Advanced Optoelectronic Quantum Architecture and Measurement (MOE), School of Physics, Beijing Institute of Technology, Beijing, China, [2]Beijing Key Laboratory of Nanophotonics and Ultrafine Optoelectronic Systems, School of Physics, Beijing Institute of Technology, Beijing, China

The study of topological semimetals has been extended to more general topological nodal systems such as metamaterials and artificial periodic structures. Among various nodal structures, triply degenerate nodal line (TDNL) is rare and, hence, has received little attention. In this work, we have proposed a simple tight-binding (TB) model, which hosts a topological non-trivial TDNL. This TDNL not only has the drumhead surface states (DSSs) as usual nodal line systems but also has surface states that form a contracted-drumhead shape. The shape and area of this contracted drumhead can be tuned by the hopping parameters of the model. This provides an effective way to modulate surface states and their density of states, which can be important in future applications of topological nodal systems.

KEYWORDS

triply degenerate nodal line, tight-binding model, drumhead surface states, Berry phase, Zak phase

1 Introduction

In recent years, topological semimetals have become a frontier topic in condensed matter physics because of their promising applications in electronics, spintronics, and optics [1–9]. According to the dimensions of the degenerate manifolds in k-space formed by band crossings, topological semimetals are divided into nodal point semimetals, such as Weyl [9–12], Dirac [13–17], or triple-point semimetals [18, 19]; nodal line semimetals [20–23]; and nodal surface semimetals [24–27]. Due to the non-trivial topological band structure, Weyl (Dirac) semimetals can exhibit Fermi arc surface states [5, 9, 10] connecting different Weyl node (Dirac node) projections on a two-dimensional (2D) surface Brillouin zone (BZ). Nodal line semimetals can exhibit another special surface state—drumhead surface state (DSS) [21, 22, 28–31] on a 2D surface BZ. These non-trivial topological properties are not limited to being present in semimetals because they originate from the nodal band structures and exist in other systems, such as metals [32–35], optical crystals [36–38], phononic crystals [39, 40], mechanical systems [41], and circuit systems [42–44].

For topological nodal line materials, the doubly degenerate Weyl nodal line [23, 45–47] and quadruply degenerate Dirac nodal line [48–51] have been broadly studied, and the DSS has been observed in these two types of materials. However, there is little research on the triply degenerate nodal line (TDNL). The only such research we can find is [52] by Liu et al.

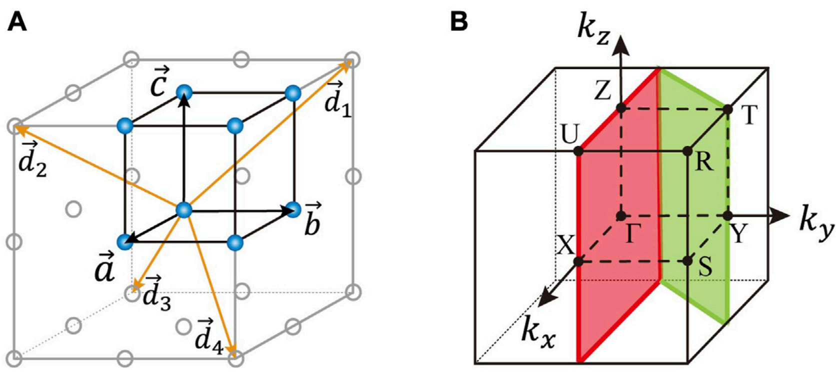

FIGURE 1
(A) Unit cell (black frame and blue balls) and hopping vectors [$\vec{a}$, $\vec{b}$, $\vec{c}$, and $\vec{d}_i$ (i = 1, 2, 3, 4)] of the model. **(B)** Bulk BZ and its projections to the (010) surface (red) and $(\bar{1}10)$ surface (green).

in 2021. Liu et al. [52] proposed two TDNL models, of which one is non-topological and the other is topological, according to the existence of Fermi arc topological surface states. However, Liu et al. did not report any DSS for the TDNL models. Accordingly, in this work, we aim to construct a tight-binding (TB) model with TDNL and investigate its DSS.

However, it is almost impossible to construct a TDNL model based on real crystalline materials because real crystalline materials are constrained by the symmetries of (magnetic) space groups, and systematic studies on the possible emergent particles from band crossings have shown that no TDNL exists under various (magnetic) space groups [53–55]. Subsequently, to construct a TDNL model, one has to get rid of the constraints by (magnetic) space groups. This can be achieved in artificial systems, such as metamaterials, circuit systems, and mechanical systems, because when described by TB models, the effective hoppings in these systems can be tuned at will, for example, adjusting the connection mode among circuit components or changing the coupling strength through springs [41, 43, 56].

In this work, we first constructed a three-band TB model hosting TDNL by designing the hoppings. Subsequently, we calculated the Berry phase and Zak phase to check the topological non-triviality of the TDNL. Surface states on two different surfaces (i.e., (010) and $(\bar{1}10)$) were studied via both semi-infinite systems and slab models. The usual DSS was found on the (010) surface. However, on the $(\bar{1}10)$ surface, we noticed a new type of DSS, whose drumhead is not complete but rather contracted. The tuning of this DSS with a contracted drumhead was also studied by varying the hopping parameters of the model.

2 Model and method

The model is constructed based on a simple cubic lattice whose basis vectors $\vec{a}$, $\vec{b}$, and $\vec{c}$ are equal in magnitude and along the x, y, and z directions, respectively, as shown in Figure 1A. Only one atom with three orbitals (here called ϕ_1, ϕ_2, and ϕ_3) is considered in each cell. With the hopping between orbitals $\phi_i(\vec{r})$ and $\phi_j(\vec{r}-\vec{\delta})$ denoted as $h_{ij}(\vec{\delta})$, we choose the following hoppings for the model:

$$h_{11}(0) = t_0,\ \ h_{22}(0) = -t_0,\ \ h_{33}(0) = 2t_0, \tag{1}$$

$$h_{11}(\pm\alpha) = \frac{t_1}{2},\ \ h_{22}(\pm\alpha) = -\frac{t_1}{2},\ \ h_{33}(\pm\alpha) = t_1, \tag{2}$$

$$h_{23}\left(\pm\vec{b}\right) = \pm\frac{t_2}{2},\ \ h_{12}\left(\pm\vec{d}_i\right) = \pm\frac{t_3}{8}\ \ (i = 1,2,3,4), \tag{3}$$

where $\alpha = \vec{a}, \vec{b}, \vec{c}$ and $\vec{d}_i$ $(i = 1, 2, 3, 4)$ are shown in Figure 1A. Then, the Hamiltonian of the TB model is

$$H = \left(t_0 + t_1\cos k_x + t_1\cos k_y + t_1\cos k_z\right)\lambda_1 + t_2\sin k_y\lambda_2 + t_3\sin k_x\sin k_y\sin k_z\lambda_3, \tag{4}$$

where λ_1, λ_2, and λ_3 are the following three matrices, respectively:

$$\begin{pmatrix} 1 & 0 & 0 \\ 0 & -1 & 0 \\ 0 & 0 & 2 \end{pmatrix},\ \begin{pmatrix} 0 & 0 & 0 \\ 0 & 0 & i \\ 0 & -i & 0 \end{pmatrix},\ \begin{pmatrix} 0 & i & 0 \\ -i & 0 & 0 \\ 0 & 0 & 0 \end{pmatrix}. \tag{5}$$

One can easily see that when $k_y = 0$, Eq. 4 becomes a diagonal matrix whose diagonal elements can be null simultaneously. This implies that a TDNL can exist in the plane $k_y = 0$ under suitable values of t_0 and t_1. The key feature of the hoppings that results in this TDNL is that $h_{ii}(0)/h_{ii}(\pm\alpha)$ keeps constant for i = 1, 2, 3. This is a special request that cannot be derived from symmetries of the (magnetic) space group.

The surface density of state (SDOS) was obtained by calculating the surface Green's function of the semi-infinite system using the WannierTools package [57]. The input data for WannierTools were prepared using the MagneticTB package [58]. To investigate the surface states, we also constructed TB slab models of 80 layers using the PythTB package [59]. To judge whether a state is a surface state, we first define the topmost five layers on each side, A or B, of the slab model as "surface layers" and then define the following quantity η to characterize the degree to which a state is a surface state:

$$\eta = \begin{cases} \left[w_{\mathrm{A}} + w_{\mathrm{B}} - \frac{1}{8}\right]\Big/\frac{7}{8}, & w_{\mathrm{A}} + w_{\mathrm{B}} > \frac{1}{8}, \\ 0, & w_{\mathrm{A}} + w_{\mathrm{B}} \le \frac{1}{8}, \end{cases} \tag{6}$$

where $w_{\mathrm{A/B}}$ represents the wavefunction weight within the surface layers of side A/B of the slab. A bulk state wavefunction is periodic, and its weights are equally distributed within all the 80 layers, in

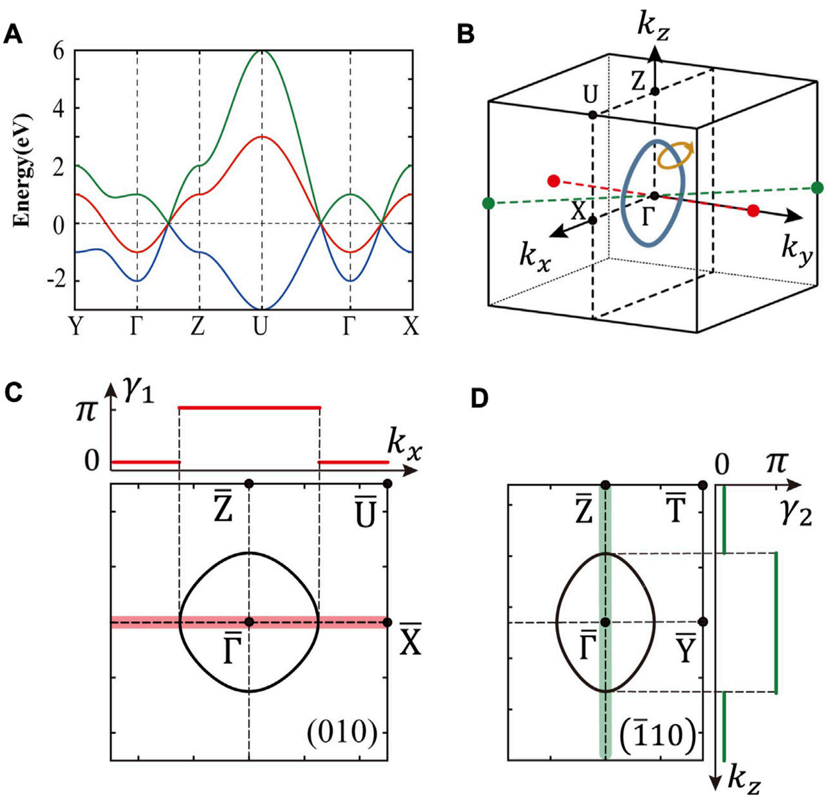

FIGURE 2
(A) Bulk band structure of the model. **(B)** TDNL (thick blue nodal ring) and the k-point path (small orange loop) for calculating the Berry phase. The red (green) dashed line is the integral path for Zak phase γ_1 at $k_x = 0$ (γ_2 at $k_z = 0$). **(C, D)** TDNL projections onto **(C)** (010) and **(D)** ($\bar{1}10$) surface BZs and the Zak phases **(C)** γ_1 (k_x) and **(D)** γ_2 (k_z).

which case $w_A = w_B = 5/80$ and $\eta = 0$. For a perfect surface state, the wavefunction is totally localized within the surface layers, leading to $w_A = w_B = 1/2$ and $\eta = 1$. By means of η, a state can be determined as a strong (or typical) surface state if its η is greater than a critical value η_c, and in this paper, $\eta_c = 0.5$ is adopted.

3 Results

If not otherwise stated, the parameters $t_0 = 2$, $t_1 = -1$, and $t_2 = t_3 = 1$ are used for the model, and the unit is eV for all energies. The bulk energy bands are shown in Figure 2A, in which the k-points are defined in Figure 1B. In this model, the TDNL is actually an approximately circular nodal ring in the $k_y = 0$ plane, as shown in Figure 2B. To check the topological properties of the TDNL, we first calculated the Berry phase defined on a closed k-point loop enclosing the TDNL, with fully gapped energies, as shown by the small orange loop in Figure 2B. The Berry phase is calculated using the Wilson loop approach [60], and the result is π, which shows the topological non-triviality of the TDNL.

Furthermore, we calculated the Zak phase [61, 62], which is the Berry phase defined in a one-dimensional BZ along a certain direction. Two Zak phases are investigated here. The first one γ_1 (k_x) is defined along the line from $(k_x, -\frac{1}{2}, 0)$ to $(k_x, \frac{1}{2}, 0)$, with the $k_x = 0$ case shown by the red dashed line in Figure 2B, in which the k-point coordinates are in unit of $2\pi/a$. The second one γ_2 (k_z) is defined along the line from $(\frac{1}{2}, -\frac{1}{2}, k_z)$ to $(-\frac{1}{2}, \frac{1}{2}, k_z)$, with the $k_z = 0$ case shown by the green dashed line in Figure 2B. The calculated Zak phase γ_1 (k_x) (γ_2 (k_z)) is shown in the top (right) panel of Figure 2C (Figure 2D), whose k_x (k_z) axis corresponds to the red (green) thick line in the 2D projective BZ of (010) ($\bar{1}10$) surface shown in the corresponding bottom (left) panel. We can see that, for both γ_1 and γ_2, the non-trivial π Zak phase emerges only when the integral path of the Zak phase traverses the nodal ring (i.e., the TDNL here). Otherwise, the Zak phase is zero. According to the bulk-edge correspondence [63], this change of topological properties from inside to outside the nodal ring implies the existence of topological surface states inside the projected nodal ring on both (010) and ($\bar{1}10$) surfaces.

The semi-infinite system terminated with that surface should be constructed to explore the topological surface states of a certain surface. Two surfaces (010) and ($\bar{1}10$) are studied here, where the (010) surface is parallel to the nodal ring, but the ($\bar{1}10$) surface is not. Figure 3A shows the SDOS of the (010) surface system, whose surface states all have a constant energy (zero) and form a flat drumhead shape. This typical DSS is clearly demonstrated by the SDOS with a constant energy slice at $E = 0$, as shown in Figure 3C. The green ring in Figure 3C represents the front projection of the TDNL, and its interior is full of surface states. We call this type of DSS "full DSS." From the result that both the Zak phases γ_1 and γ_2 equal π inside the TDNL projections, one may expect that full DSS also exists in the ($\bar{1}10$) surface system. However, the SDOS of the ($\bar{1}10$) surface system shown in Figures 3B, D demonstrates results

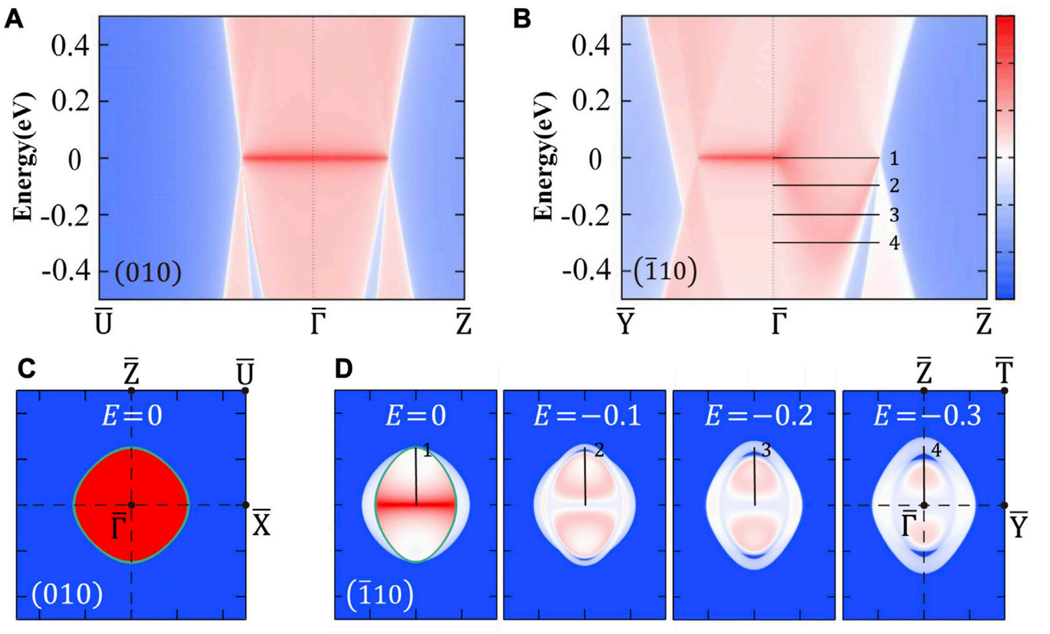

FIGURE 3
Topological surface states given by SDOS for the semi-infinite systems terminated with **(A, C)** (010) and **(B, D)** $(\bar{1}10)$ surfaces. **(A, B)** Continuous energy resolved SDOS. **(C)** Constant energy slice at E = 0 for the (010) surface system. **(D)** Constant energy slices at E = 0, −0.1, −0.2, −0.3 for the $(\bar{1}10)$ surface system, in which the cutting lines 1–4 correspond to those in **(B)**. The green lines in **(C, D)** are the projections of the TDNL.

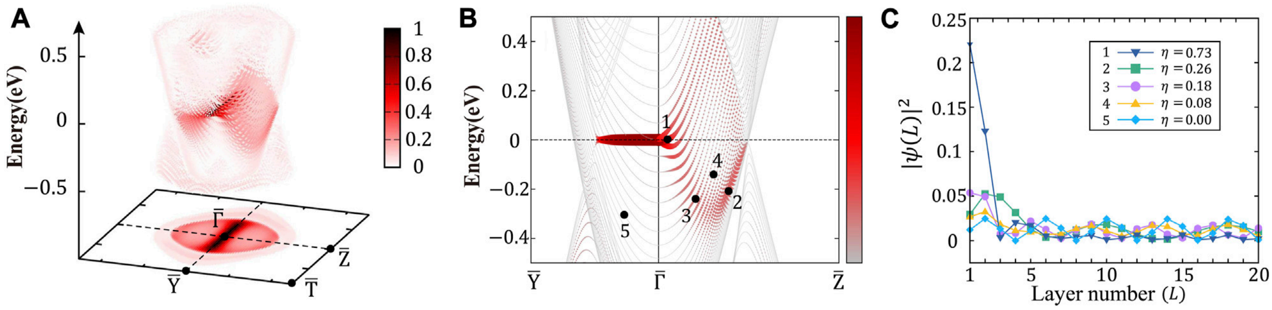

FIGURE 4
$(\bar{1}10)$ slab model. **(A)** Distribution of η (the degree of surface state) represented by color for all states with energy in the range [−0.5, 0.5]. The largest η at each k-point is also projected onto the surface BZ. **(B)** Energy bands with η represented by both color and point size. **(C)** Squared wavefunctions with respect to the layer number (only 20 out of the total 80 layers are shown) for the five states marked in **(B)**.

different from the expectation. In particular, the leftmost panel of Figure 3D shows the "contracted-drumhead surface state (CDSS)," in which the surface states do not fill completely the interior of the TDNL oblique projection (the green ellipse). The weak surface state feature at other energies, as shown in other panels of Figure 3D, also supports this result.

In order to further explore the CDSS in the $(\bar{1}10)$ surface system, a slab model of 80 layers terminated with $(\bar{1}10)$ surface is studied. Its energy bands are shown in Figure 4B, in which the degree of surface state η defined in Eq. 6 is also shown by both the point size and color for each state. In addition, Figure 4A shows the distribution of η for all states within the energy range [−0.5, 0.5] in the whole surface BZ and the projection of η onto the surface BZ. Figure 4B corresponds to Figure 3B, but here we can access the wavefunction of any state of the slab model. The wavefunctions of the five states marked in Figure 4B have descending η from 0.73 to 0, and the distributions of their weights with respect to layer number are given in Figure 4C. We can see that state 1 with η = 0.73 is a strong surface state with most wavefunctions localized within the surface layers. At the other extreme, state 5 with η = 0 distributes periodically; hence, it is a bulk state. As for states 2–4, they have non-zero but small η. Although they contain surface state components or may be called weak surface states, they are more like bulk states. Figures 4A, B show that strong surface states exist only near zero energy. Consequently, even if the projection of η in Figure 4A selects the largest η for each k-point within the energy range [−0.5, 0.5], it is not much different from the

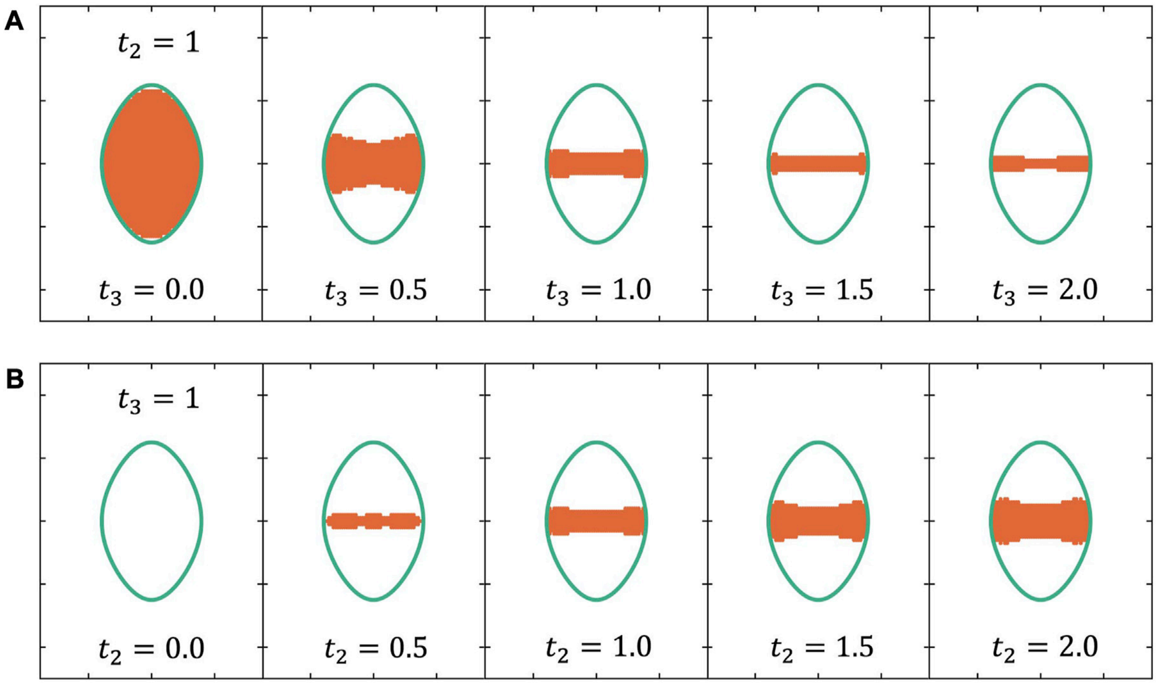

FIGURE 5
k-point distribution (orange area) of the CDSS for the $(\bar{1}10)$ slab model with different parameters. **(A)** $t_3 = 0, 0.5, 1.0, 1.5, 2.0$ with $t_2 = 1.0$. **(B)** $t_2 = 0, 0.5, 1.0, 1.5, 2.0$ with $t_3 = 1.0$. The green ellipse denotes the projection of the TDNL. The other two parameters are $t_0 = 2$ and $t_1 = -1$ for all cases.

case considering only zero energy, and it exhibits a similar shape to the $E = 0$ panel in Figure 3D.

Because the weak surface states are much like bulk states, they are not efficient in most applications, which require large SDOS. Thus, only strong surface states need to be considered, and the shape of the CDSS can be revealed by the distribution of the k-points at which strong surface states exist. Figure 5 shows the distribution of the k-points of strong surface states (i.e., the shape of CDSS) under different model parameters. We can see that the shape of CDSS for the $(\bar{1}10)$ surface can be tuned by the hoppings t_2 and t_3 efficiently. Namely, increasing t_3 makes the surface states change from a full DSS to a CDSS with smaller areas (Figure 5A), and inversely, increasing t_2 will increase the area of CDSS from zero (Figure 5B). This provides an effective route to tune the SDOS and the shape of the surface state in topological nodal systems.

4 Conclusion

We have proposed a simple TB model hosting TDNL and studied its topological properties. Both the Berry phase and Zak phase demonstrate that the TDNL is topological non-trivial. This TDNL model not only has a full DSS as usual topological nodal line systems, but also has a CDSS, which we first noticed. The CDSS exists on the $(\bar{1}10)$ surface, and its area can be tuned efficiently by both model parameters t_2 and t_3. Our model demonstrates an effective way to tune the amount and density of the surface states, which will expand the potential applications of topological nodal line systems.

Data availability statement

The original contributions presented in the study are included in the article/Supplementary Material. Further inquiries can be directed to the corresponding author.

Author contributions

G-BL supervised the project and guided the work. Y-RW performed the calculations and wrote the manuscript. G-BL revised the manuscript. All authors contributed to the article and approved the submitted version.

Funding

This work was supported by the National Natural Science Foundation of China with Grant Nos 12274028, 52161135108, and 12234003 and the National Key R&D Program of China with Grant No. 2022YFA1402603.

Conflict of interest

The authors declare that the research was conducted in the absence of any commercial or financial relationships that could be construed as a potential conflict of interest.

Publisher's note

References

1. Bansil A, Lin H, Das T. Colloquium: topological band theory. *Rev Mod Phys* (2016) 88:021004. doi:10.1103/RevModPhys.88.021004

2. Weng HM, Dai X, Fang Z. Topological semimetals predicted from first-principles calculations. *J Phys Condens Matter* (2016) 28:303001. doi:10.1088/0953-8984/28/30/303001

3. Burkov AA, Hook MD, Balents L. Topological nodal semimetals. *Phys Rev B* (2011) 84:235126. doi:10.1103/PhysRevB.84.235126

4. Yan BH, Felser C. Topological materials: Weyl semimetals. *Annu Rev Conden Matter Phys* (2017) 8:337–54. doi:10.1146/annurev-conmatphys-031016-025458

5. Hasan MZ, Xu SY, Belopolski I, Huang SM. Discovery of weyl fermion semimetals and topological fermi arc states. *Annu Rev Conden Matter Phys* (2017) 8:289–309. doi:10.1146/annurev-conmatphys-031016-025225

6. Witczak-Krempa W, Chen G, Kim YB, Balents L. Correlated quantum phenomena in the strong spin-orbit regime. *Annu Rev Conden Matter Phys* (2014) 5:57–82. doi:10.1146/annurev-conmatphys-020911-125138

7. Bernevig BA, Felser C, Beidenkopf H. Progress and prospects in magnetic topological materials. *Nature* (2022) 603:41–51. doi:10.1038/s41586-021-04105-x

8. Lv BQ, Qian T, Ding H. Experimental perspective on three-dimensional topological semimetals. *Rev Mod Phys* (2021) 93:025002. doi:10.1103/RevModPhys.93.025002

9. Wan X, Turner AM, Vishwanath A, Savrasov SY. Topological semimetal and fermi-arc surface states in the electronic structure of pyrochlore iridates. *Phys Rev B* (2011) 83:205101. doi:10.1103/PhysRevB.83.205101

10. Weng HM, Fang C, Fang Z, Bernevig BA, Dai X. Weyl semimetal phase in noncentrosymmetric transition-metal monophosphides. *Phys Rev X* (2015) 5:011029. doi:10.1103/PhysRevX.5.011029

11. Xu SY, Belopolski I, Alidoust N, Neupane M, Bian G, Zhang C, et al. Discovery of a weyl fermion semimetal and topological fermi arcs. *Science* (2015) 349:613–7. doi:10.1126/science.aaa9297

12. Xu SY, Alidoust N, Belopolski I, Yuan Z, Bian G, Chang TR, et al. Discovery of a weyl fermion state with fermi arcs in niobium arsenide. *Nat Phys* (2015) 11:748–54. doi:10.1038/nphys3437

13. Wang Z, Sun Y, Chen XQ, Franchini C, Xu G, Weng H, et al. Dirac semimetal and topological phase transitions in A_3Bi(A=Na, K, Rb). *Phys Rev B* (2012) 85:195320. doi:10.1103/physrevb.85.195320

14. Wang Z, Weng H, Wu Q, Dai X, Fang Z. Three-dimensional Dirac semimetal and quantum transport in Cd_3As_2. *Phys Rev B* (2013) 88:125427. doi:10.1103/physrevb.88.125427

15. Liu ZK, Zhou B, Zhang Y, Wang ZJ, Weng HM, Prabhakaran D, et al. Discovery of a three-dimensional topological Dirac semimetal, Na_3Bi. *Science* (2014) 343:864–7. doi:10.1126/science.1245085

16. Liu ZK, Jiang J, Zhou B, Wang ZJ, Zhang Y, Weng HM, et al. A stable three-dimensional topological Dirac semimetal Cd_3As_2. *Nat Mater* (2014) 13:677–81. doi:10.1038/nmat3990

17. Neupane M, Xu SY, Sankar R, Alidoust N, Bian G, Liu C, et al. Observation of a three-dimensional topological Dirac semimetal phase in high-mobility Cd_3As_2. *Nat Comms* (2014) 5:3786. doi:10.1038/ncomms4786

18. Lv BQ, Feng ZL, Xu QN, Gao X, Ma JZ, Kong LY, et al. Observation of three-component fermions in the topological semimetal molybdenum phosphide. *Nature* (2017) 546:627–31. doi:10.1038/nature22390

19. Ma JZ, He JB, Xu YF, Lv BQ, Chen D, Zhu WL, et al. Three-component fermions with surface fermi arcs in tungsten carbide. *Nat Phys* (2018) 14:349–54. doi:10.1038/s41567-017-0021-8

20. Fang C, Chen Y, Kee HY, Fu L. Topological nodal line semimetals with and without spin-orbital coupling. *Phys Rev B* (2015) 92:081201. doi:10.1103/PhysRevB.92.081201

21. Huang H, Liu J, Vanderbilt D, Duan W. Topological nodal-line semimetals in alkaline-earth stannides, germanides, and silicides. *Phys Rev B* (2016) 93:201114. doi:10.1103/physrevb.93.201114

22. Xu Q, Yu R, Fang Z, Dai X, Weng H. Topological nodal line semimetals in the CaP_3 family of materials. *Phys Rev B* (2017) 95:045136. doi:10.1103/PhysRevB.95.045136

23. Chen W, Lu HZ, Hou JM. Topological semimetals with a double-helix nodal link. *Phys Rev B* (2017) 96:041102. doi:10.1103/PhysRevB.96.041102

24. Wu W, Liu Y, Li S, Zhong C, Yu ZM, Sheng XL, et al. Nodal surface semimetals: theory and material realization. *Phys Rev B* (2018) 97:115125. doi:10.1103/physrevb.97.115125

25. Fu BB, Yi CJ, Zhang TT, Caputo M, Ma JZ, Gao X, et al. Dirac nodal surfaces and nodal lines in ZrSiS. *Sci Adv* (2019) 5:eaau6459. doi:10.1126/sciadv.aau6459

26. Yang Y, ping Xia J, xiang Sun H, Ge Y, Jia D, qi Yuan S, et al. Observation of a topological nodal surface and its surface-state arcs in an artificial acoustic crystal. *Nat Commun* (2019) 10:5185. doi:10.1038/s41467-019-13258-3

27. Chen SZ, Li S, Chen Y, Duan W. Nodal flexible-surface semimetals: case of carbon nanotube networks. *Nano Lett* (2020) 20:5400–7. doi:10.1021/acs.nanolett.0c01786

28. Weng HM, Liang YY, Xu QN, Yu R, Fang Z, Dai X, et al. Topological node-line semimetal in three-dimensional graphene networks. *Phys Rev B* (2015) 92:045108. doi:10.1103/PhysRevB.92.045108

29. Chan YH, Chiu CK, Chou MY, Schnyder AP. Ca_3P_2 and other topological semimetals with line nodes and drumhead surface states. *Phys Rev B* (2016) 93:205132. doi:10.1103/PhysRevB.93.205132

30. Bian G, Chang TR, Zheng H, Velury S, Xu SY, Neupert T, et al. Drumhead surface states and topological nodal-line fermions in$TlTaSe_2$. *Phys Rev B* (2016) 93:121113. doi:10.1103/physrevb.93.121113

31. Belopolski I, Manna K, Sanchez DS, Chang G, Ernst B, Yin J, et al. Discovery of topological weyl fermion lines and drumhead surface states in a room temperature magnet. *Science* (2019) 365:1278–81. doi:10.1126/science.aav2327

32. Xu SY, Liu C, Kushwaha SK, Sankar R, Krizan JW, Belopolski I, et al. Observation of fermi arc surface states in a topological metal. *Science* (2015) 347:294–8. doi:10.1126/science.1256742

33. Wang Z, Gresch D, Soluyanov AA, Xie W, Kushwaha S, Dai X, et al. $MoTe_2$: A type-II weyl topological metal. *Phys Rev Lett* (2016) 117:056805. doi:10.1103/physrevlett.117.056805

34. Zhu Z, Winkler GW, Wu Q, Li J, Soluyanov AA. Triple point topological metals. *Phys Rev X* (2016) 6:031003. doi:10.1103/physrevx.6.031003

35. Sun JP, Zhang D, Chang K. Coexistence of topological nodal lines, weyl points, and triply degenerate points in TaS. *Phys Rev B* (2017) 96:045121. doi:10.1103/physrevb.96.045121

36. Gao W, Yang B, Tremain B, Liu H, Guo Q, Xia L, et al. Experimental observation of photonic nodal line degeneracies in metacrystals. *Nat Commun* (2018) 9:950. doi:10.1038/s41467-018-03407-5

37. Yang B, Guo Q, Tremain B, Liu R, Barr LE, Yan Q, et al. Ideal weyl points and helicoid surface states in artificial photonic crystal structures. *Science* (2018) 359:1013–6. doi:10.1126/science.aaq1221

38. Wang L, Jian SK, Yao H. Topological photonic crystal with equifrequency weyl points. *Phys Rev A* (2016) 93:061801. doi:10.1103/physreva.93.061801

39. Li F, Huang X, Lu J, Ma J, Liu Z. Weyl points and fermi arcs in a chiral phononic crystal. *Nat Phys* (2017) 14:30–4. doi:10.1038/nphys4275

40. Zhang T, Song Z, Alexandradinata A, Weng H, Fang C, Lu L, et al. Double-weyl phonons in transition-metal monosilicides. *Phys Rev Lett* (2018) 120:016401. doi:10.1103/physrevlett.120.016401

41. Ma GC, Xiao M, Chan CT. Topological phases in acoustic and mechanical systems. *Nat Rev Phys* (2019) 1:281–94. doi:10.1038/s42254-019-0030-x

42. Lu YH, Jia NY, Su L, Owens C, Juzeliunas G, Schuster DI, et al. Probing the berry curvature and fermi arcs of a weyl circuit. *Phys Rev B* (2019) 99:020302. doi:10.1103/PhysRevB.99.020302

43. Lee CH, Imhof S, Berger C, Bayer F, Brehm J, Molenkamp LW, et al. Topolectrical circuits. *Commun Phys* (2018) 1:39. doi:10.1038/s42005-018-0035-2

44. Luo K, Yu R, Weng H. Topological nodal states in circuit lattice. *Research* (2018) 2018:6793752. doi:10.1155/2018/6793752

45. Feng BJ, Zhang RW, Feng Y, Fu BT, Wu SL, Miyamoto K, et al. Discovery of weyl nodal lines in a single-layer ferromagnet. *Phys Rev Lett* (2019) 123:116401. doi:10.1103/PhysRevLett.123.116401

46. Liu LL, Wang CZ, Li JX, Chen XQ, Jia Y, Cho JH. Two-dimensional topological semimetal states in monolayer Cu_2Ge, Fe_2Ge, and Fe_2Sn. *Phys Rev B* (2020) 101:165403. doi:10.1103/PhysRevB.101.165403

47. Chen C, Yu ZM, Li S, Chen ZY, Sheng XL, Yang SA. Weyl-loop half-metal in $Li_3(FeO_3)_2$. *Phys Rev B* (2019) 99:075131. doi:10.1103/PhysRevB.99.075131

48. Kim Y, Wieder BJ, Kane CL, Rappe AM. Dirac line nodes in inversion-symmetric crystals. *Phys Rev Lett* (2015) 115:036806. doi:10.1103/PhysRevLett.115.036806

49. Nakhaee M, Ketabi SA, Peeters FM. Dirac nodal line in bilayer borophene: tight-binding model and low-energy effective Hamiltonian. *Phys Rev B* (2018) 98:115413. doi:10.1103/PhysRevB.98.115413

50. Li RH, Ma H, Cheng XY, Wang SL, Li DZ, Zhang ZY, et al. Dirac node lines in pure alkali earth metals. *Phys Rev Lett* (2016) 117:096401. doi:10.1103/PhysRevLett.117.096401

51. Mullen K, Uchoa B, Glatzhofer DT. Line of Dirac nodes in hyperhoneycomb lattices. *Phys Rev Lett* (2015) 115:026403. doi:10.1103/PhysRevLett.115.026403

52. Liu ZH, Wang LY, Yao DX. Triply degenerate nodal lines in topological and nontopological metals. *Phys Rev B* (2021) 103:205145. doi:10.1103/PhysRevB.103.205145

53. Yu ZM, Zhang Z, Liu GB, Wu W, Li XP, Zhang RW, et al. Encyclopedia of emergent particles in three-dimensional crystals. *Sci Bull* (2022) 67:375–80. doi:10.1016/j.scib.2021.10.023

54. Liu GB, Zhang Z, Yu ZM, Yang SA, Yao Y. Systematic investigation of emergent particles in type-III magnetic space groups. *Phys Rev B* (2022) 105:085117. doi:10.1103/PhysRevB.105.085117

55. Zhang Z, Liu GB, Yu ZM, Yang SA, Yao Y. Encyclopedia of emergent particles in type-IV magnetic space groups. *Phys Rev B* (2022) 105:104426. doi:10.1103/physrevb.105.104426

56. Luo KF, Yu R. Topological states in electric circuit. *Acta Phys Sin* (2019) 68:220305. doi:10.7498/aps.68.20191398

57. Wu QS, Zhang SN, Song HF, Troyer M, Soluyanov AA. Wanniertools: an open-source software package for novel topological materials. *Comput Phys Commun* (2018) 224:405–16. doi:10.1016/j.cpc.2017.09.033

58. Zhang ZY, Yu ZM, Liu GB, Yao YG. Magnetictb: A package for tight-binding model of magnetic and non-magnetic materials. *Comput Phys Commun* (2022) 270:108153. doi:10.1016/j.cpc.2021.108153

59. Coh S, Vanderbilt D. *Python tight binding (PythTB)* (2012). Available from: http://www.physics.rutgers.edu/pythtb.

60. Wang HX, Guo GY, Jiang JH. Band topology in classical waves: Wilson-loop approach to topological numbers and fragile topology. *New J Phys* (2019) 21:093029. doi:10.1088/1367-2630/ab3f71

61. Zak J. Berry's phase for energy bands in solids. *Phys Rev Lett* (1989) 62:2747–50. doi:10.1103/PhysRevLett.62.2747

62. Xiao D, Chang MC, Niu Q. Berry phase effects on electronic properties. *Rev Mod Phys* (2010) 82:1959–2007. doi:10.1103/RevModPhys.82.1959

63. Rhim JW, Behrends J, Bardarson JH. Bulk-boundary correspondence from the intercellular Zak phase. *Phys Rev B* (2017) 95:035421. doi:10.1103/physrevb.95.035421